Journal of Nuclear Materials 202 (1993) 104–121
North-Holland

journal of nuclear materials

Irradiation assisted stress corrosion cracking of controlled purity 304L stainless steels

J.M. Cookson [a], R.D. Carter Jr. [a], D.L. Damcott [a], M. Atzmon [a] and G.S. Was [b]

[a] *Department of Nuclear Engineering, and* [b] *Department of Nuclear Engineering and Department of Materials Science and Engineering, The University of Michigan, Ann Arbor, MI 48109, USA*

Received 27 July 1992; accepted 11 December 1992

The effect of chromium, phosphorus, silicon and sulfur on the stress corrosion cracking of 304L stainless steel in CERT tests in high purity water or argon at 288°C following irradiation with 3.4 MeV protons at 400°C to 1 dpa, has been investigated using ultrahigh purity alloys (UHP) with controlled impurity additions. Grain boundary segregation of phosphorus or silicon due to proton irradiation was quantified using both Auger electron spectroscopy and scanning transmission electron microscopy, and the alloys with impurity element additions were observed to have greater grain boundary chromium depletion and nickel enrichment than the UHP alloy. The UHP alloy suffered severe cracking in CERT tests in water. Less cracking was found after CERT tests of irradiated UHP+P or UHP+Si alloys, despite greater chromium depletion. This suggests a mitigating effect of phosphorus and silicon at grain boundaries. No cracking was found in argon tests, eliminating a purely mechanical embrittlement mechanism, but not eliminating a contribution from radiation hardening. Implanted hydrogen was not a factor in the intergranular cracking found.

1. Introduction

Irradiation assisted stress corrosion cracking (IASCC) has been described as the accelerated intergranular cracking of materials exposed to ionizing radiation [1,2], and is a major concern in light water reactors around the world. While the mechanism by which this cracking occurs has not been established, the growing body of research concerning IASCC has identified some of the major material and environmental factors which are involved. Much research has been conducted to characterize the role of environmental factors, principally oxygen concentration, electrochemical potential, and impurity ion concentration, on the crack propagation rate in furnace sensitized austenitic stainless steel at high temperature [3–5]. However, the difficulty, expense, and time required to test neutron irradiated specimens has meant that the stress corrosion cracking consequences of radiation induced microstructural and microcompositional changes have yet to be extensively investigated.

The microstructural and microchemical features, or persistent effects due to neutron exposure, can be modeled by other forms of radiation such as heavy ions, helium, and protons in much less time and with little or no sample activation. Studies of stainless steel specimens irradiated with 5 MeV or 46.5 MeV nickel ions examined radiation damage and radiation induced segregation [6,7]. However, because of the limited ion range (1–5 μm), the effect of radiation on intergranular SCC could not be studied in specimens with grain sizes similar to commercial alloys (20–30 μm). Other work using up to 60 MeV helium ions has induced IASCC in specimens 400 μm thick [8], but the considerable irradiation time required and the residual activity induced by these irradiations complicate this technique and make it less viable to gather the large number of data points required to systematically study IASCC.

In contrast to these methods of irradiating stainless steel, 3.4 MeV protons induce nearly uniform damage along 38 μm of the 43 μm range (with the nonuniform end of range damage concentrated in a 5 μm wide peak), and are inexpensive to perform. With a grain size of approximately 10 μm, 3.4 MeV protons penetrate roughly 4 to 6 grains with a fairly uniform displacement rate. The energy of the ions is low enough to keep the activation of the specimens to levels at

which no special handling is required. As with other types of ion irradiation [6,7], the temperature at which the proton irradiations are conducted must be greater than that of neutron irradiation in order for the rate of thermal processes to match the higher displacement rate of the incident protons compared to that of neutrons. Thus, an irradiation time on the order of 20–60 h is required to reach the displacements per atom (dpa) range of interest in light water reactor cores. In this way the microstructural features of an in-core irradiated stainless steel specimen can be modeled validly at a fraction of the time and cost.

Modeling microstructural features is an essential part of studying irradiation assisted stress corrosion cracking, as the persistent effects of neutron irradiation have important implications for the stress corrosion cracking susceptibility of irradiated stainless steels [1,2]. These effects include the redistribution of elements at the grain boundaries, principally chromium depletion and impurity enrichment due to vacancy and interstitial defect fluxes, and the hardening of the microstructure due to the formation of dislocation loops and other extended defects. A great deal of research has identified grain boundary chromium depletion due to precipitation of chromium carbides during thermal treatments as the dominant cause of stress corrosion cracking in unirradiated stainless steel [9–12]; as a result, the depletion of chromium at grain boundaries due to irradiation is regarded as very significant [1,2]. A threshold minimum grain boundary chromium concentration of 14.0 wt% (15 at%) in thermally treated 304 stainless steel was identified by Bruemmer et al. [9] above which little IGSCC occurred. However, extrapolating these results to irradiated material is limited by both the difference between the grain boundary depletion width of irradiated stainless steel compared with thermally treated stainless steel, and the simultaneous hardening of irradiated stainless steel [1,2]. Thus, the effect of chromium depletion in IASCC has to be examined with irradiated specimens. Studies using specimens irradiated in-core have found grain boundary chromium depletion from 18.8 wt% (20.0 at%) to 15.8 wt% (16.8 at%) at a fluence of approximately 1×10^{25} neutrons/m^2 ($E > 1$ MeV) [13,14]. As a fluence of 0.7×10^{25} neutrons/m^2 ($E > 1$ MeV) has been correlated with a damage level of 1 displacement per atom (dpa) [1], this corresponds to a damage level of approximately 1.5 dpa. Studies using irradiated specimens indicate a possible relationship between depletion and IASCC [13–17], but isolating the effect of chromium depletion in irradiated specimens is complicated by both impurity segregation and radiation hardening which occur along with chromium depletion. Consequently, no studies have unequivocally assessed the degree to which chromium depletion is important in the IASCC process.

Studies of unirradiated stainless steel have shown that the enrichment of impurity elements such as phosphorus and/or sulfur at the grain boundary due to irradiation may be important in IASCC. The thermal segregation of phosphorus and sulfur in stainless steel to grain boundary concentrations higher than those found in radiation-induced segregation studies caused little increase in intergranular cracking in phosphorus-doped alloys, greater intergranular cracking in sulfur-doped alloys, and low levels of IG cracking in alloys doped with both sulfur and phosphorus, in high temperature, pH = 2.5 water [4,5]. Experiments in boiling concentrated nitric acid linked both phosphorus and sulfur to greater environmental cracking [18]. Studies using irradiated specimens have not resolved how SCC behaviour is modified by grain boundary impurity enrichment [8,16,17] due to irradiation. Some direct comparisons between high purity and commercial purity heats have been made, but the results are rather contradictory, partially due to unsystematic composition variations in the original materials. After CERT tests performed in high temperature, high purity water on 304 stainless steel specimens irradiated with 60 MeV helium ions between 288 and 300°C to a damage level of 0.4 dpa, Fukuya et al. [8] found greater elongation at failure for the two specimens doped with phosphorus than for the undoped specimens. Our previously reported work [19] found a similar effect of phosphorus in high purity 304 stainless steel alloys irradiated with 3.4 MeV protons at 400°C to 1 dpa. However, further work to examine the nature of the effect of phosphorus identified in these preliminary studies is necessary. No systematic investigations regarding the possible role of sulfur in IASCC have been reported.

As silicon does not segregate thermally, the only studies assessing the role of grain boundary enrichment of silicon involve irradiation [1]. While silicon has been observed to enrich at the grain boundaries under neutron irradiation, and after nickel ion irradiation [7,13,14,16], the effects of its presence are uncertain. Jacobs et al. [16] found that neutron irradiated commercial-purity specimens were somewhat more likely to crack than high-purity specimens and attributed this difference to the presence of silicon, which was the most significant difference between the grain boundary compositions of the commercial and high purity heats. However, they subsequently reported no direct correlation between cracking and silicon enrichment [14].

Table 1
Chemical composistion of the UHP 304L stainless steel alloys as reported by GE and analyzed by electron microprobe

Alloy [a]	Cr	Ni	Mo	Si	Mn	C	N	P	S
UHP									
GE wt% [at%]	19.2 [20.4]	9.03 [8.5]	< 0.005 [< 0.003]	0.03 [0.06]	1.11 [1.11]	0.0046 [0.021]	0.0031 [0.012]	< 0.005 [< 0.009]	0.005 [0.0086]
probe wt% [at%]	19.5 [20.72]	9.43 [8.88]	–	0.05 [0.09]	1.11 [1.11]	–	–	0.006 [0.01]	–
UHP + P									
GE wt% [at%]	18.5 [19.7]	9.5 [9.0]	< 0.005 [< 0.003]	0.02 [0.04]	1.15 [1.16]	0.0015 [0.0069]	0.0022 [0.009]	0.059 [0.105]	0.006 [0.0095]
probe wt% [at%]	19.8 [21.02]	9.22 [8.68]	–	0.02 [0.03]	1.14 [1.15]	–	–	0.046 [0.08]	–
UHP + S									
GE wt% [at%]	18.7 [19.9]	8.9 [8.4]	< 0.005 [< 0.003]	< 0.01 [< 0.02]	1.06 [1.07]	0.0015 [0.0069]	0.0034 [0.013]	< 0.005 [< 0.009]	0.019 [0.033]
probe wt% [at%]	19.7 [20.91]	9.49 [8.94]	–	0.02 [0.03]	1.03 [1.04]	–	–	–	–
UHP + Si									
GE wt% [at%]	19.1 [20.4]	9.02 [8.5]	< 0.005 [< 0.003]	0.46 [0.91]	1.16 [1.17]	0.0011 [0.0051]	0.0022 [0.009]	< 0.005 [< 0.009]	0.004 [0.0074]
probe wt% [at%]	19.2 [20.41]	9.08 [8.55]	–	0.44 [0.87]	1.33 [1.34]	–	–	–	–
UHP + C									
GE wt% [at%]	18.5 [19.7]	9.5 [8.9]	–	–	1.2 [1.21]	0.03 [0.138]	0.03 [0.119]	–	–

[a] Balance iron.

Fukuya et al. [8], in experiments performed with 60 MeV helium ions between 288 and 300°C to a damage level of 0.4 dpa, found that their high purity material was more susceptible to cracking than their commercial purity material, which contained ten times more silicon. Other work by Chung et al. [17] with both high purity and commercial purity neutron-irradiated material found that the commercial purity material showed greater time to failure in slow strain rate tests than the high purity specimens. While the phosphorus and sulfur compositions of the commercial purity material were not available, the silicon composition was reported, and was two orders of magnitude higher than that of the high purity alloy. No systematic studies isolating the role of silicon on IASCC susceptibility have been reported.

The work reported here examines the role of chromium, phosphorus, sulfur, and silicon on intergranular SCC in high purity water or argon at 288°C following proton irradiation of ultra high purity 304L stainless steel and ultra high purity 304L stainless steel doped with impurity elements. By using alloys with controlled impurity content, the role of each impurity element on IASCC can be isolated. Irradiations were conducted at 400°C to a calculated damage level of 1 dpa in the uniform damage region. The elevated irradiation temperature of 400°C was chosen to offset the elevated displacement rate of protons compared to neutrons, and was based on the theoretically determined relationship between temperature and displacement rate [1,20]. Specimens were examined using scanning Auger electron spectroscopy (AES) and scanning transmission electron microscopy with energy dispersive spectroscopy (STEM/EDS) to quantify the radiation-induced changes in grain boundary composition, and transmission electron microscopy (TEM) to evaluate the radiation-induced microstructural features. The observations are correlated with results from constant extension rate tensile (CERT) tests in high temperature water.

2. Experimental

2.1. Materials

The alloys investigated were ultrahigh purity (UHP) type 304L stainless steel and UHP heats doped with 600 wppm (0.11 at%) phosphorus (UHP + P), 200 wppm (0.03 at%) sulfur (UHP + S), 4600 wppm (0.9 at%) silicon (UHP + Si) and 300 wppm (0.14 at%) carbon (UHP + C) supplied by The General Electric Co. The base compositions of these alloys, as reported by General Electric and as determined by electron microprobe analysis, are shown in table 1. The alloys were received as approximately 10 mm thick bars and were solution annealed at 1100°C for 1 h to homogenize the microstructure and microchemistry, with a resulting grain size of approximately 100–200 μm. These bars were sectioned and then cold rolled to form plates approximately 30 mm wide and either 4 mm or 2 mm thick. The 4 mm plates were machined into SCC specimens with a gage section 32 mm long, 2 mm wide and 1.5 mm thick, then mechanically polished using a Dremel™ hand grinder to 2400 grit, (which led to variations of up to 5% in the cross sectional area along the gage length) prior to final annealing. The SCC specimen geometry is shown in fig. 1. The 2 mm thick plates were cut into specimens 2 mm wide for Auger specimens, or 4 mm wide for TEM specimens and then wet polished to 2400 grit prior to final annealing. The final annealing treatment in a flowing argon atmosphere at 850°C for 1 h (UPH, UHP + Si) or 0.5 h (UHP + P, UPH + S) recrystallized the alloys to achieve grain sizes of approximately 10 μm. After annealing, all specimens were mechanically repolished with 2400 grit paper and electropolished using a solution of 60% phosphoric acid, 40% sulfuric acid at a voltage of 7 to 8 V for 5 min. The UHP + C alloy was rolled from 10 mm barstock to 4 mm, machined to the same SCC specimen geometry, solution annealed at 1100°C for 1 h, and subsequently heat treated at 650°C for 25 h to induce severe grain boundary chromium depletion due to the formation of chromium carbides. The same mechanical repolish and electropolish treatment was performed on this specimen as for the other specimens, but it was not irradiated.

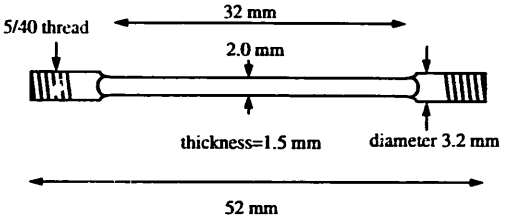

Fig. 1. Schematic of the SCC test specimens.

2.2. Proton irradiation

Irradiation using 3.4 MeV protons were carried out in a specially designed stage connected to the General

Ionex Tandetron in the Michigan Ion Beam Laboratory at the University of Michigan. The specimens were mounted on a copper block with a thin foil of tin between the specimens and the stage, which was subsequently melted to provide good thermal contact. The nominal temperature of the irradiated surface of the specimens during irradiation was 400 ± 10°C, as monitored via an infrared pyrometer which could be remotely controlled to scan across the irradiated region, thus ensuring temperature uniformity. The pyrometer was calibrated prior to the irradiation using four thermocouples spot welded to the unirradiated regions of the specimens. The temperature of the irradiation was controlled by simultaneously heating the stage from the rear with an electric heating element and cooling the stage with flowing air, as shown in fig. 2. These irradiations, conducted at a pressure below 2×10^{-8} Torr, produced a nearly uniform region of damage over the first 38 μm of the 43 μm proton range, as calculated by TRIM90 [21], shown in fig. 3. The total dose was 1 dpa, with a dose rate in the uniform region of approximately 7×10^{-6} dpa/s at the nominal current density of 0.1 μA/mm^2, resulting in an irradiation time of approximately 40 h. The incident proton beam

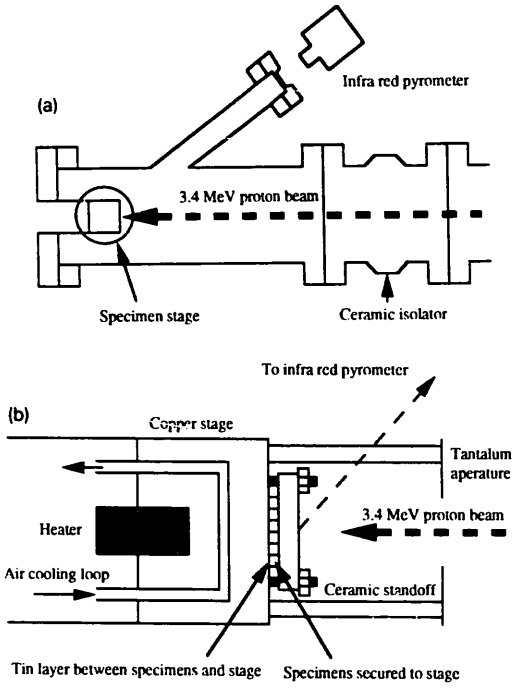

Fig. 2.(a) The controlled temperature stage used for proton irradiations. (b) Detail of the controlled temperature irradiation stage in (a).

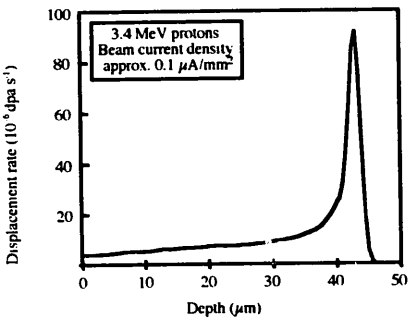

Fig. 3. The damage profile of 3.4 MeV protons in stainless steel with a nominal beam current density of 0.1 μA/mm^2 as calculated by TRIM90 [20].

was focused down to a spot approximately 6 mm in diameter with an intensity of approximately 40 μA, and then rastered across the specimens. Half of the beam was overscanned onto a tantalum aperture, resulting in a 10 mm by 16 mm uniformly irradiated region on the specimens. No visible surface changes were observed. Subsequent post-irradiation beta particle counting using a Tennelec LB 5100 automated alpha/beta counter was used to ensure the uniformity of the irradiation across all of the specimens. The specific activity of these specimens typically varied by less than 8% for a 7-sample irradiation. Any tin remaining on the unirradiated side of the SCC specimens was removed by mechanical polishing and electropolishing for 3 min using the previously mentioned solution. This final electropolish removed approximately 10–15 μm from the irradiated surface, reducing the thickness of the irradiated region from 40 μm to between 25–30 μm.

2.3. Auger electron spectroscopy

Auger electron spectroscopy (AES) was performed to quantify grain boundary composition following irradiation of the UHP, UHP + P and UHP + S alloys. Samples were cathodically charged with hydrogen following the procedure of Briant [22] and fractured in situ in a Perkin Elmer (PHI) 660 scanning Auger microprobe chamber at approximately 0°C by bending the specimens at a slow rate so that the samples failed after approximately 5 min. Intergranular fracture was achieved to a depth of approximately 40 μm on the irradiated face of all alloys except UHP + Si, and also on the unirradiated face of the UHP + P alloy. As the UHP + Si specimens could not be fractured intergranularly, no Auger analysis was performed on this alloy.

Spectra of intensity versus Auger electron energy were initially collected in survey mode to identify all of the elements present on the exposed grain boundaries. Subsequent data was acquired using multiplex mode, scanning only the energy intervals of the elemental peaks. The iron, chromium and nickel peaks were collected for all the alloys analyzed, with the peaks for phosphorus or sulfur included as well for the UHP + P or UHP + S doped alloys, respectively. Contamination by carbon and oxygen was monitored continuously throughout the data acquisition by including the elemental peaks for both elements in the multiplexed acquisitions. Data collection was terminated when the carbon and/or oxygen peaks became distinguishable from the background noise, with estimated concentrations below 5 at%. All spectra were acquired using a beam energy of 10 keV and a current of 5 nA at a pressure below 7×10^{-9} Torr. Auger spectra were converted to atomic concentrations using a standard routine which normalized peak heights and accounted for the Auger electron sensitivities of each element of interest [23]. Details of the experimental procedure have been described previously [24,25].

2.4. Transmission electron microscopy

Three-millimeter disk samples for STEM analysis were cut from the irradiated specimens using a slurry drill core cutter, mechanically back-thinned to a thickness of approximately 100 μm, and then thinned to electron transparency by jet polishing. The solution used for jet thinning was 80% ethanol, 20% perchloric acid at a constant voltage of 120 V and a temperature of −55°C. Microstructural analysis was performed using a JEOL 2000FX STEM/TEM, a Philips EM420 TEM, and a Philips CM12 STEM/TEM at the University of Michigan Electron Microbeam Analysis Laboratory (EMAL). Microchemical analysis via STEM was performed on a Philips EM400T-FEG/STEM at Oak Ridge National Laboratory. EDS analysis in the EM400T-FEG used a 2 nm incident probe in STEM mode in regions of the sample less than 100 nm thick. The grain boundary compositions were determined by averaging at least 12 measurements for each irradiated specimen. In addition, composition profiles of each element were determined across two grain boundaries which displayed significant segregation.

Microstructural analysis was performed using standard techniques to determine the dislocation network density, the dislocation loop size and character, loop density, and the black dot density. The details of these analyses have been described previously [25].

2.5. Constant extension rate tensile tests

High temperature constant extension rate tensile (CERT) test were conducted to evaluate the SCC behavior of the specimens. These tests were performed in a titanium autoclave capable of straining four specimens in parallel, which provided identical conditions within a given test. The load on each specimen was independently monitored. Except for the first test series, samples tested in the CERT setup together were irradiated together. In our notation, the irradiation batch number follows the sample designation; UHP/X for batch X. When two or more specimens from the same heat were irradiated together, a letter follows the designation, e.g., UHP/Xa, UHP/Xb. CERT experiments in water were performed at 288°C with an initial strain rate of 3.6×10^{-7} s^{-1}. The dissolved oxygen concentration was 2 ppm for all but the first and second tests and was controlled by continuously bubbling a mixture of 5% oxygen in argon through a glass mixing column, which acted as the water reservoir. Inlet and outlet conductivity were monitored and controlled via automatic additions of dilute sulfuric acid so that the outlet conductivity was maintained at 0.5 μS/cm. The solution was deionized and then returned to the mixing reservoir to minimize wastage. The setup is shown in fig. 4. The corrosion potential was not monitored during these experiments, but is estimated +150 mV_{SHE} based on the relationship between the solution conductivity, oxygen concentration, and electrochemical potential for type 304 stainless steel in 288°C water [1].

The conditions in the water tests were chosen to provide an environment which was aggressive enough

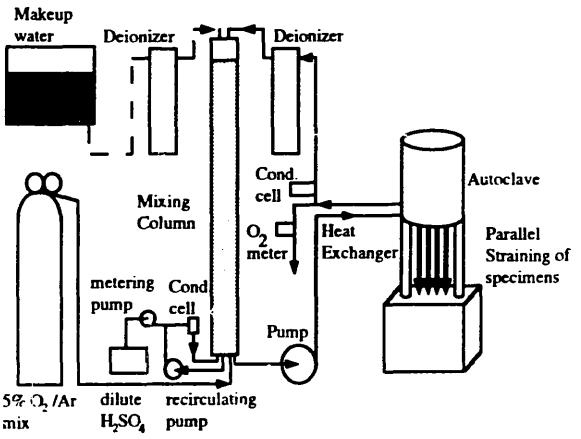

Fig. 4. Schematic of the CERT test facility.

to achieve a sufficient degree of discrimination between microstructures. A preliminary experiment to establish the severity of the water environment was performed on a UHP + C specimen in the unirradiated, sensitized condition. CERT tests were also performed in argon at 288°C in the same autoclave with an initial strain rate of 3.6×10^{-7} s^{-1} to evaluate the role of the environment on the observed cracking, while two specimens were tested in room temperature air at an initial strain rate of 3.6×10^{-6} s^{-1} to evaluated the role of injected hydrogen on the observed cracking.

After each CERT test was completed, the fracture surface, the irradiated surface and the unirradiated surfaces of each specimen were examined for evidence of intergranular cracking. Comparison between the irradiated face and the unirradiated face of the specimens were significant as these surface were identical apart from the irradiation, so that any differences could be directly attributed to the irradiation. The susceptibility of the irradiated specimens to IASCC was assessed via the number of cracks in the irradiated region, the elongation at failure, the location and mode of failure, and the prominence of slip steps in the irradiated region.

3. Results

3.1. Microchemical analysis

The results of both the Auger and the STEM/EDS analysis are presented in table 2. The number of measurements per sample, number of samples and number of irradiation batches for these samples are given in this table for each alloy and condition analyzed. Significant amounts of chromium depletion and nickel enrichment were observed at the grain boundaries in all the irradiated alloys. Auger results revealed grain boundary chromium depletion from the bulk concentration (as determined by microprobe) of 20.7 at% to 17.2 at% in the UHP alloy, while grain boundary depletion from 21.0 at% to 15.0 at% was found in the irradiated UHP + P alloy and from 20.9 at% to 15.0 at% in the irradiated UHP + S alloy. Phosphorus enrichment to 5.3 at% was observed on the unirradiated UHP + P grain boundaries and 8.7 at% on the irradiated UHP + P grain boundaries. The phosphorus enrichment on the unirradiated boundaries resulted from the recrystallization anneal at 850°C. In the UHP + S specimens, on only 3 out of the 41 boundaries examined was sulfur segregation observed (to approx. 1.6 at%).

The STEM/EDS measurements confirmed the trend found via Auger for the UHP and the UHP + P irradiated alloys, with less grain boundary chromium depletion from the bulk concentration (20.7 at% to an average of 17.3 at%) found for the irradiated UHP specimen than the chromium depletion (21.0 at% to an average of 16.5 at%) found for the irradiated UHP + P specimen. The STEM/EDS grain boundary profiles for the irradiated UHP + Si specimen indicate a grain boundary chromium depletion from the bulk concentration of 20.4 at% to an average of 14.4 at%. Impurity segegation was found in both alloys with elevated impurity element concentrations; phosphorus segregation

Table 2
Summary of the grain boundary compositions of the UHP, UHP + P, UHP + Si and UHP + S alloys after irradiation, as determined by either Auger or STEM, in atomic percent. Errors are given as the standard deviation of the mean [a]

Alloy	Analysis method	Number of measurements	Number of samples	Number of batches	Iron	Chromium	Nickel	Phosphorus	Sulfur	Silicon
UHP irrad.	Auger	31	5	3	69.9±0.7	17.2±0.7	12.9±0.3	ND	ND	ND
UHP irrad.	STEM/EDS	26	2	2	71.5±0.3	17.1±0.1	11.0±0.2	ND	ND	ND
UHP + P unirrad.	Auger	8	4	2	64.3±1.0	21.7±0.7	8.8±0.5	5.3±0.4	ND	ND
UHP + P irrad.	Auger	34	7	3	62.5±0.7	15.0±0.4	13.8±0.5	8.7±0.4	ND	ND
UHP + P irrad.	STEM/EDS	12	1	1	68.7±0.2	17.1±0.4	12.4±0.3	1.8±0.1	ND	ND
UHP + Si irrad.	STEM/EDS	27	1	1	69.7±0.2	14.8±0.2	12.8±0.3	ND	ND	3.2±0.2
UHP + S irrad.	Auger	42	5	2	69.3±0.5	15.0±0.5	15.5±0.5	ND	ND	ND
UHP + S irrad.	STEM/EDS	18	1	1	71.4±0.2	16.1±0.2	12.0±0.2	ND	ND	ND

[a] ND: none detected.

to 1.4 at% in the UHP + P specimen, and silicon segregation to 3.2 at% in the UHP + Si specimen. The average of the two grain boundary profiles determined from two boundaries with significant segregation in each of the irradiated UHP, UHP + P and UHP + Si specimens are shown in fig. 5. The deviations from the bulk compositions at the grain boundary for the alloys as determined via both Auger and STEM/EDS are shown in fig. 6.

3.2. Microstructural analysis

The unirradiated microstructures were very similar to each other, with average grain diameters of 10–12 μm for the UHP alloy, 7–9 μm for the UHP + P, UHP + S and UHP + Si alloy, which did not change under irradiation. Before irradiation the network dislocation density was 1.6×10^{13} m^{-2} in the UHP alloy, and approximately the same in the UHP + P, UHP + S alloys and UHP + Si alloys. No dislocation loops were present before irradiation. A typical microstructure of the annealed specimens is shown in fig. 7a. The observed microstructural changes due to irradiation are summarized in table 3. The dislocation microstructure was dramatically affected by the irradiation, as shown in fig. 7b. After irradiation the network densities increased to 2×10^{14} m^{-2} (UHP), 2×10^{14} m^{-2} (UHP + P), 2×10^{13} m^{-2} (UHP + S) and 1×10^{14} m^{-2} (UHP + Si). The dislocation loop densities were 6×10^{21} m^{-3} (UHP and UHP + P), 9×10^{21} m^{-3} (UHP + S), and 1×10^{22} m^{-3} (UHP + Si) after irradiation. Eighty five percent of the loops were faulted with $\boldsymbol{b} = \frac{1}{3}\langle 111 \rangle$. The remainder were unfaulted perfect loops with $\boldsymbol{b} = \frac{1}{2}\langle 110 \rangle$. The average faulted loop sizes were 16 nm (UHP), 27 nm (UHP + P), 14 nm (UHP + S), and 10 nm (UHP + Si). Only interstitial loops were observed. Black-dot damage was observed in all the irradiated alloys, with densities of 7×10^{21} m^{-3} (UHP), 8×10^{21} m^{-3} (UHP + P), 9.6×10^{21} m^{-3} (UHP + S), and 1.3×10^{21} m^{-3} (UHP + Si).

No voids were seen in any of the irradiated specimens. TEM also revealed two precipitate types that were present in all samples: spinel and an Fe–Cr rich particle. These particles were present in the as-received material, were not removed by the solution

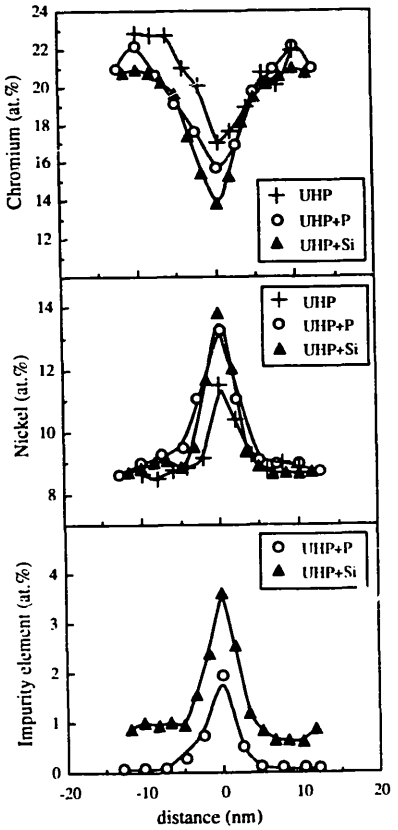

Fig. 5. Grain boundary composition profiles for th UHP, UHP + P and UHP + Si alloys after 3.4 MeV proton irradiation at 400°C to a damage level of 1 dpa, determined by STEM/EDS.

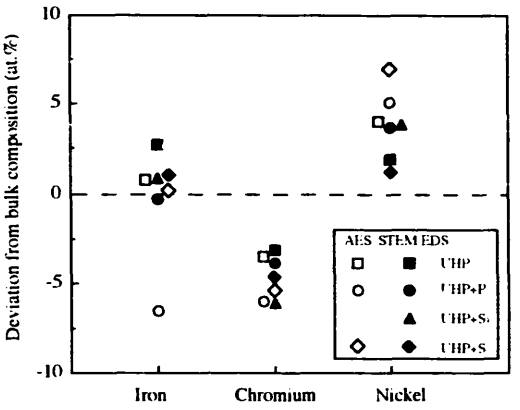

Fig. 6. Deviation in the major element grain boundary compositions from the bulk (as determined by electron microprobe) for the UHP, UHP + P, UHP + Si and UHP + S alloys after 3.4 MeV proton irradiation at 400°C to a damage level of 1 dpa, determined by both Auger and STEM/EDS. (All values shown here are raw measurements.) Note that the trends in the segregation behavior identified by Auger are confirmed by STEM/EDS, although the magnitudes vary.

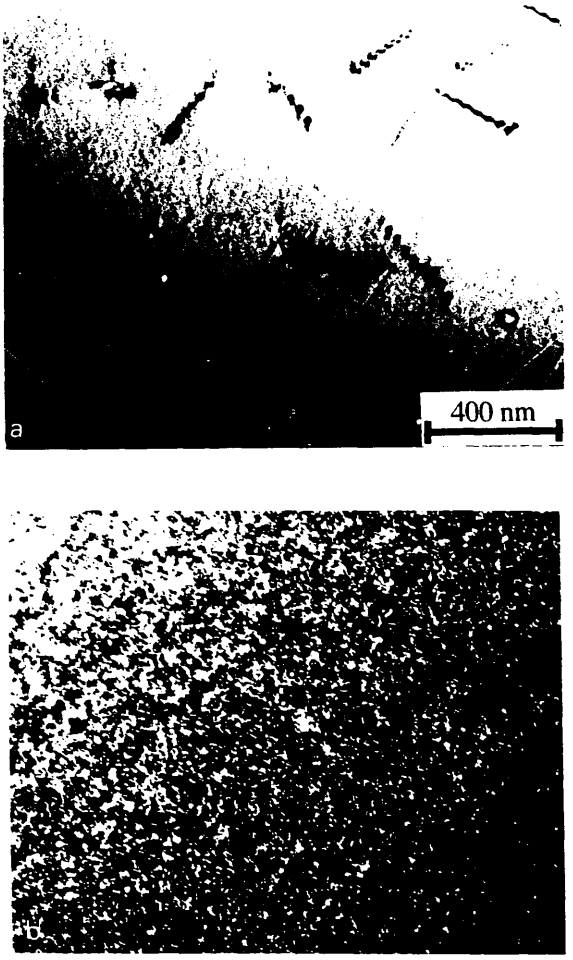

Fig. 7.(a) Bright field TEM micrograph of the dislocation morphology in the UHP + P alloy after annealing at 850°C for 0.5 h. (b) Bright field TEM micrograph of the dislocation morphology in the UHP + Si alloy after annealing at 850°C for 1 h followed by irradiation with protons at 400°C to 1 dpa.

anneal and were not affected by irradiation. As discussed in reference [25], these microstructural features are consistent with those reported in other microstructural studies of stainless steel irradiated with neutrons to comparable damage levels and at temperatures similar to light water reactors.

3.3. IASCC experiments

3.3.1. Water tests

The first test was conducted on a highly sensitized (650°C/25 h) carbon containing specimen, UHP + C to verify the aggresiveness of the sample-environment combination, for which many results exist [1,9–12]. The test resulted in complete intergranular fracture of the UHP + C specimen at a strain of 11%. This test was conducted simultaneously with a UHP specimen, which remained uncracked to a strain of 18%, at which point the test was stopped.

A total of five CERT tests on two to three samples per test were conducted in water using UHP, UHP + P, UHP + S and UHP + Si alloys originating from five separate proton irradiations. A summary of the results of the CERT tests is shown in table 4. In each test, the irradiated UHP specimens demonstrated significantly more intergranular cracking than the irradiated UHP + P, UHP + S or UHP + Si specimens, as shown in fig. 8. An average of 20 intergranular cracks extending across the specimen were found in the irradiated region of the four UHP specimens tested in the 0.5 μS/cm conductivity water, while 23 transverse intergranular cracks were found in the irradiated region of the UHP/3 specimen tested in 0.25 μS/cm water. The lower conductivity apparently had little impact on the number of intergranular cracks in the irradiated region of specimen UHP/3.

The irradiated volume had little reduction in area

Table 3
Summary of the microstructural features observed in the UHP, UHP + P, UHP + Si and UHP + S irradiated alloys after 3.4 MeV proton irradiation at 400°C to 1 dpa

Alloy	Grain size (μm)	Network density (m^{-2})	Loop type	Loop density (m^{-3})	Faulted loop size (nm)	Black dot density (m^{-3})	Precipitates present
UHP unirrad.	10 to 12	1.6×10^{13}	None	None	None	None	Spinel, α-ferrite
UHP irrad.	10 to 12	2.2×10^{14}	85% faulted	5.6×10^{21}	16 ± 9	6.7×10^{21}	Spinel, α-ferrite
UHP + P irrad.	7 to 9	2.0×10^{14}	85% faulted	5.7×10^{21}	27 ± 13	8.0×10^{21}	Spinel, α-ferrite
UHP + Si irrad.	7 to 9	9.8×10^{13}	85% faulted	1.0×10^{22}	10 ± 7	1.3×10^{22}	Spinel, α-ferrite
UHP + S irrad.	7 to 9	2.0×10^{13}	85% faulted	9.4×10^{21}	14 ± 8	9.6×10^{21}	Spinel, α-ferrite

Table 4
Summary of the CERT tests performed

Specimen	Irrad. number	CERT number	Environment [a]	Elongation at failure (%)	Number of IG cracks in irradiated region	Location of failure [b]	Slip step formation [c]
UHP+C sens	Unirrad.	1	Water	11.5	Unirrad.	Central	
UHP unirrad	Unirrad.	1	Water	18	Unirrad.	Test halted	
UHP unirrad	Unirrad.	2	Water	23	Unirrad.	Ends	
UHP/2	2	5	Water	13.4	24	Irradiated region	2
UHP/3	3	6	Water (0.25)	16.5	23	Irradiated region	2
UHP/4a	4	7 [d]	Water	12.6	14	Irradiated region	2
UHP/5	5	8	Water	13.1	20	Irradiated region	2
UHP/6	6	9	Water	13.1	18	Irradiated region	2
UHP+P/2	2	5	Water	18	10	Irradiated region	3
UHP+P/3	3	6	Water (0.25)	23	1	Unirrad region	3
UHP+P/4	4	7 [d]	Water	28	1	Unirrad region	3
UHP+P/5	5	8	Water	25	5	Unirrad region	3
UHP+S/3	3	6	Water (0.25)	12.7	1	Irradiated region	2
UHP+S/4	4	7 [d]	Water	23	1	Unirrad region	3
UHP+S/5	5	8	Water	11.6	2	Irradiated region	2
UHP+Si/6a	6	9	Water	27	3	Unirrad region	4
UHP+Si/6b	6	9	Water	25	4	Unirrad region	4
UHP unirrad.	Unirrad.	10	Argon	25	Unirrad.	Ends	1
UHP/4b	4	10	Argon	27	None	Unirrad	4
UHP/7a	7	11	Argon	22	None	Unirrad	4
UHP+P/7	7	11	Argon	25	None	Unirrad	4
UHP unirrad.	Unirrad.	12	25°C air	51	Unirrad.	Ends	Not resolvable
UHP/7b	7	12	25°C air	48	None	Unirrad	Not resolvable

[a] Water tests: 288°C water at 0.5 μS/cm (unless noted), 2 ppm oxygen conc., at an initial strain rate of $3.6\ 10^{-7}$/s; argon tests: 288°C purified argon, at an initial strain of 3.6×20^{-7}/s; 25°C air tests: room temperature air at initial strain rate of 3.6×10^{-6}/s.
[b] All samples which failed in the irradiated region had IG cracking which led to sample failure.
[c] Slip step formation: 1 = very small, 4 = very pronounced.
[d] CERT test held at high temperature for 300 h before straining.

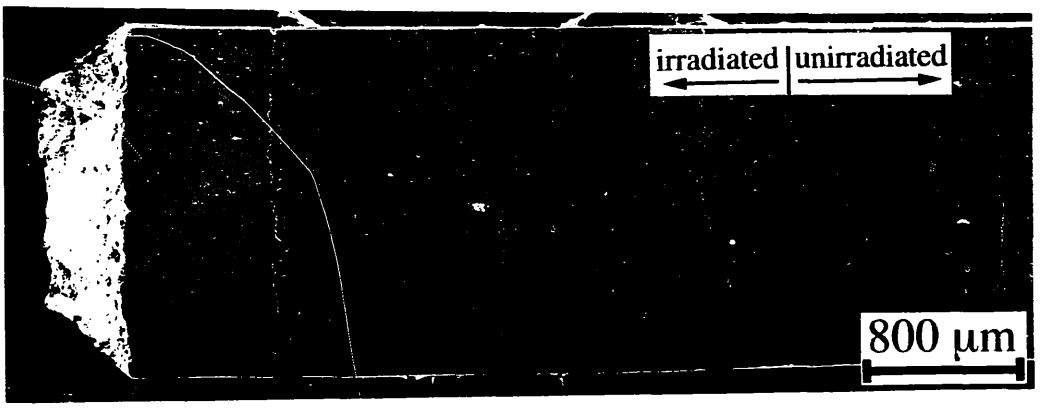

Fig. 8. Typical surface of a specimen (UHP/4a) irradiated with 3.4 MeV protons at 400°C to 1 dpa, after a CERT test in 2 ppm water at 288°C with an initial strain rate of $3.6\times10^{-7}\ s^{-1}$. A total of 14 intergranular cracks were found in both halves of the irradiated region, and none in the unirradiated region.

compared to the unirradiated volume of the specimen, which resulted in distortion of the fracture surface as shown in fig. 9a. Intergranular cracking within 25–30 μm of the surface was found in the irradiated region, corresponding to the thickness of the irradiated region following electropolishing, as shown in fig. 9b. Beyond this intergranular region, transgranular cracking occurred, followed by ductile, dimpled fracture where final overload took place.

The stress-strain curves from the CERT tests of the irradiated and unirradiated UHP specimens in fig. 10a indicate a consistent elongation at failure of approximately 13% for four irradiated UHP specimens tested in 0.5 μS/cm conductivity water. Specimen UHP/3, tested in water with a conductivity of 0.25 μS/cm had an elongation at failure of 17%. The unirradiated UHP specimen failed at 23% elongation, and no cracking was found on the surface of this specimen.

The amount of cracking found in the irradiated UHP + P specimens was significantly lower than that of the irradiated UHP specimens. The stress-strain curves from the CERT tests of the irradiated UHP + P specimens in fig. 10b indicate that of the four irradiated UHP + P specimens, three had elongations of 23% to 27%, comparable to the unirradiated UHP specimen tested in water. Although there were be-

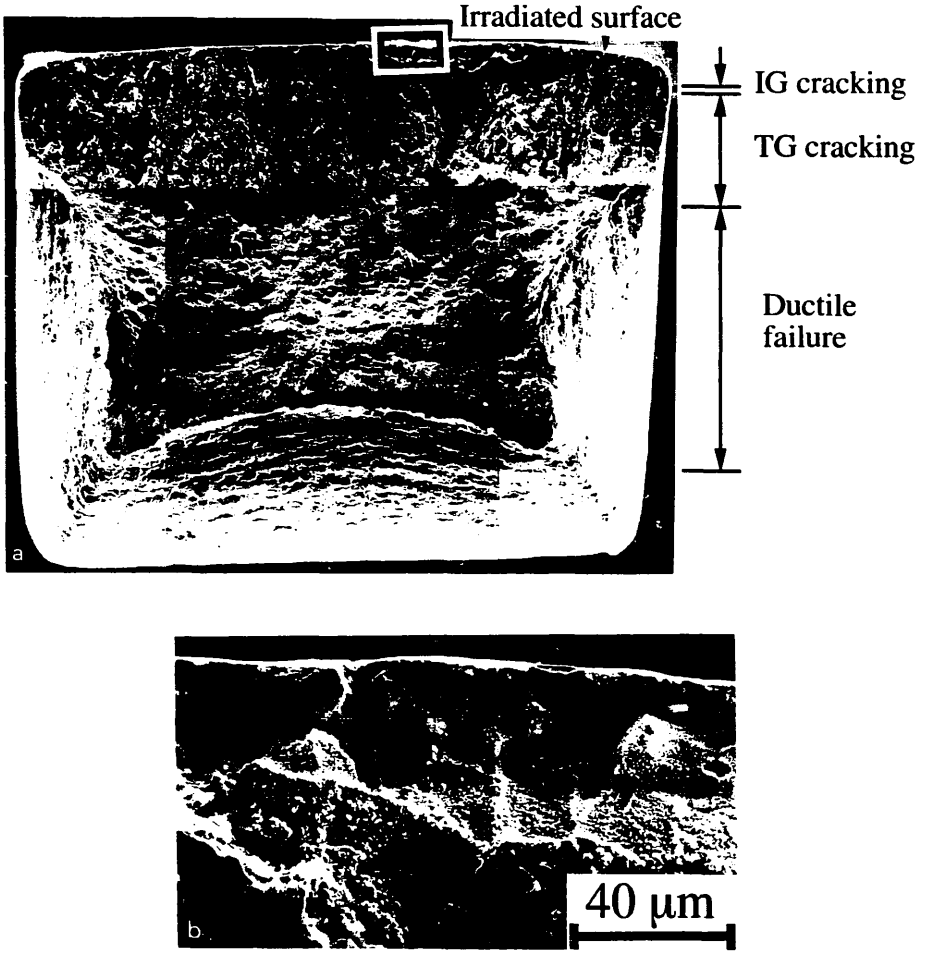

Fig. 9.(a) Fracture surface of a specimen (UHP/3) irradiated with 3.4 MeV protons at 400°C to 1 dpa, which failed below 20%, after a CERT test in 2 ppm O_2 water at 288°C with an initial strain rate of 3.6×10^{-7} s^{-1}. Intergranular cracks were initiated in the irradiated region, and propagated as transgranular cracks through the bulk, leading to ductile failure. (b) Enlargement of the fracture surface in (a) which revealed intergranular cracking in the irradiated region, corresponding to the 43 μm range of the protons, less the 10 to 15 μm removed via electropolishing.

tween one and five intergranular cracks in the irradiated region of these specimens, none failed in the irradiated region. The remaining specimen UHP + P/2 failed significantly below the elongation at failure of 23% for the unirradiated UHP CERT test. This specimen had ten cracks in the irradiated region, one of which propagated and led to failure.

The two irradiated UHP + Si specimens tested together in water failed at elongations of 25 to 27%, greater than that of the unirradiated UHP specimen as shown in the stress strain curves in fig. 10c. Although both had three or fe - intergranular cracks in the irradiated region, these cracks did not propagate, and neither of these specimens failed in the irradiated region.

The cracking susceptibility of the UHP + S specimens was difficult to characterize from our tests. The stress-strain curves for the irradiated UHP + S specimen CERT tests in fig. 10d indicate rather inconsistent results in terms of the elongation at failure. Two specimens failed within the irradiated region at less than 13% elongation, but specimen UHP + S/4 failed outside the irradiated region at 23% elongation. This test was complicated because the sample was kept at the test conditions for approximately 300 h (due to difficulties with the equipment) prior to straining and oxide ledges consistent with spalling of oxide film were found on both ends of the UHP + S/4 specimen after the test, while the intergranular crack observed was filled with oxide. Hence, oxidation may have been a factor with the UHP + S/4 specimen. In all three of the irradiated UHP + S specimens tested, the number of intergranular cracks in the irradiated region was low, either one or two. This contrasted with the average of 20 at comparable strains in the irradiated region of the UHP specimen.

Within each alloy group, both the number of cracks and the elongation at failure fell within a small range of values, as shown in fig. 11. The exception to this was the large range of the elongation to failure of the three irradiated UHP + S specimens. With the exception of the two UHP + S specimens which failed at low elon-

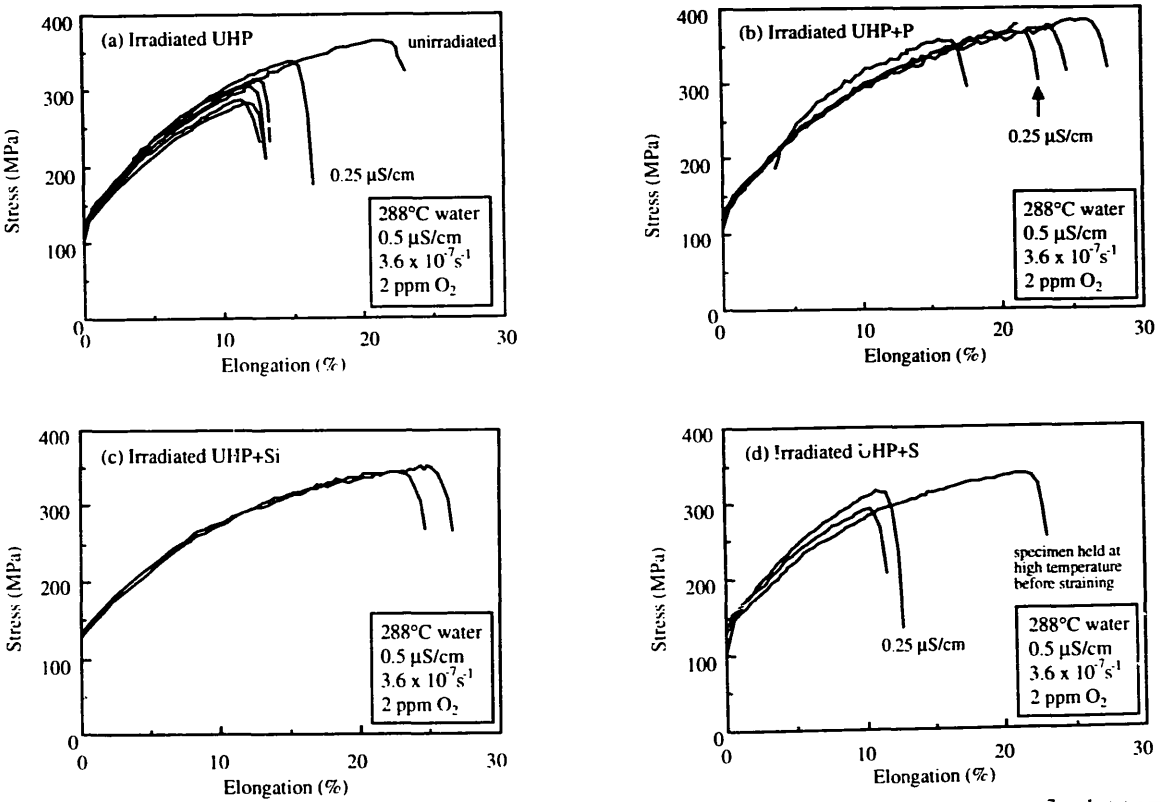

Fig. 10. Stress strain curves from CERT tests in 288°C water with 2 ppm O_2 with an initial strain rate of 3.6×10^{-7} s^{-1}. (a) UHP, (b) UHP + P, (c) UHP + Si, and (d) UHP + S.

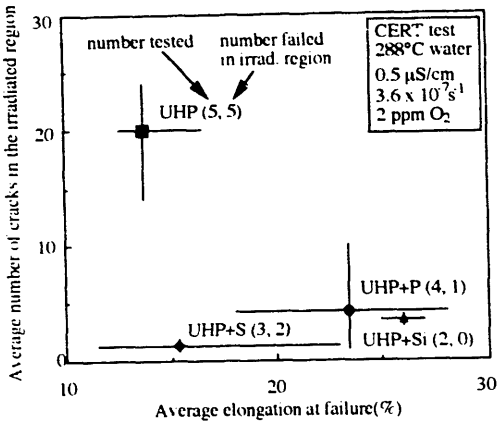

Fig. 11. Average number of cracks versus average elongation at failure for the UHP, UHP+P, UHP+Si and UHP+S specimens irradiated with 3.4 MeV protons at 400°C to 1 dpa then CERT tested in 0.5 μS/cm, 2 ppm O_2 water at 288°C with an initial strain rate of 3.6×10^{-7} s^{-1}. The lines cover the range of the number of cracks and the elongation at failure for all specimens from a given alloy. The number of irradiated specimens tested, and the number which failed in the irradiated region from each alloy follows the alloy label.

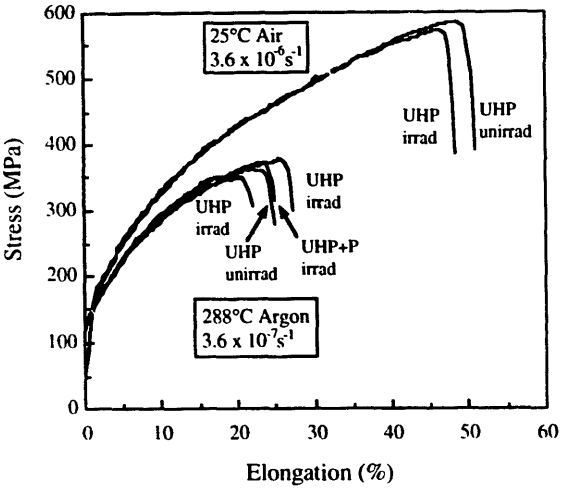

Fig. 12. Stress strain curves from the CERT tests, irradiated UHP and UHP+P and unirradiated UHP in argon with an initial strain rate of 3.6×10^{-7} s^{-1}, and irradiated and unirradiated UHP in room temperature air with an initial strain rate of 3.6×10^{-6} s^{-1}.

gations, the number of cracks found in the irradiated region of the CERT specimens tested in water decreased with increasing elongation at failure. Both reduction in elongation at failure and the number of cracks indicate susceptibility of an irradiated alloy to SCC.

3.3.2. *Inert environment tests*

Three CERT tests on samples originating from two irradiations were conducted in inert environments, two in 288°C argon, and one in room temperature air. No cracking was found on *any* specimens tested in 288° argon, whether irradiated or unirradiated. The results of these CERT tests are summarized in table 4. The stress-strain curves, shown in fig. 12, indicate that the elongations at failure for all these specimens exceeded

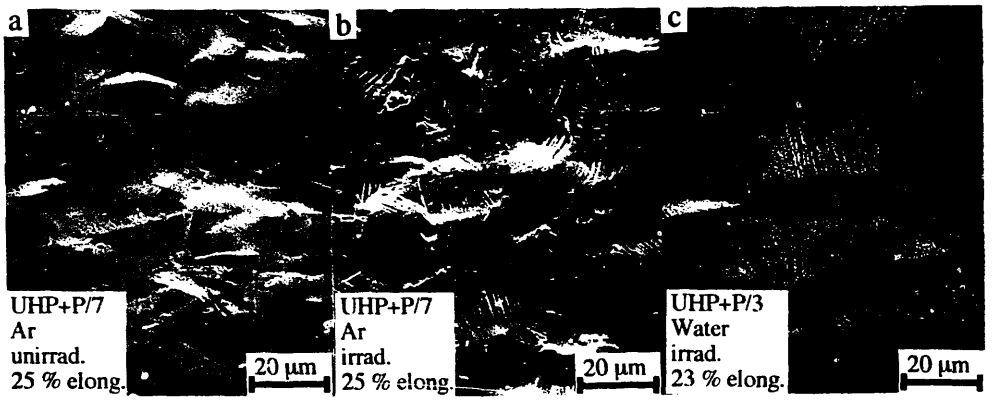

Fig. 13. Surface slip behavior following CERT tests in 2 ppm O_2 water at 288°C with an initial strain rate of 3.6×10^{-7} s^{-1}; (a) unirradiated region of UHP+P/7 in argon 25% elongation at failure; (b) irradiated region of UHP+P/7 in argon, 25% elongation at failure; and (c) irradiated region of UHP+P/3 in water, 23% elongation at failure.

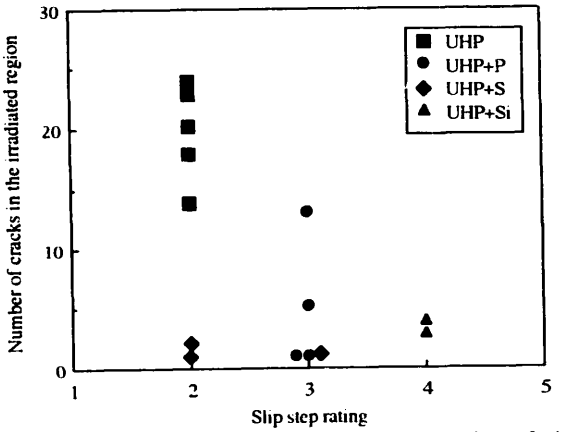

Fig. 14. Number of cracks present in the region of the specimens irradiated with 3.4 MeV protons at 400°C to 1 dpa after CERT tests in 2 ppm O_2 at 288°C water with an initial strain rate of 3.6×10^{-7} s^{-1}, versus the degree of deformation (as slip step coarseness rating, 1 = very fine, 4 = very pronounced).

22% and averaged 25%, comparable to the elongation at failure of 23% for the unirradiated UHP specimen tested in water. The irradiated specimen UHP/4b tested in argon had been irradiated along with UHP/4a, which cracked severely in the CERT test under identical conditions except for the presence of the water.

No intergranular cracking was observed on either the irradiated or the unirradiated specimens strained simultaneously at an initial strain rate of 3.6×10^{-6} s^{-1} in room temperature air. The stress-strain curves for these specimens, shown in fig. 12, indicate elongations at failure exceeding 45% for both specimens. After testing, these two specimens were highly magnetizable, as opposed to all of the specimens tested at elevated temperatures, indicating that substantial transformation to martensite had occurred due to the low temperature straining of this specimen.

3.3.3. Surface features of deformed irradiated specimens

The specimen surface in the unirradiated regions of all irradiated specimens roughened as deformation proceeded, typified by the uneven surface of the UHP + P /7 specimen tested in argon, shown in fig. 13a. However, the hardening due to irradiation led to concentrated slip and the formation of slip steps as well as surface roughening in the irradiated region of the same specimen, as shown in fig. 13b. These features were less distinct due to the presence of oxide on the specimens tested in water, but were still resolvable, as shown in fig. 13c. The prominence of slip steps was characterized (1 = very small and 4 = very pronounced), on the irradiated surface of the specimens tested, and negative correlation was found with the number of cracks present, as shown in fig. 14. The greater the deformation in the irradiated region, as indicated by how pronounced the slip steps were, the lower the number of cracks present. Again, the two irradiated UHP + S specimens which cracked at low elongations were the exception to this correlation.

4. Discussion

The most important result from this study is the observation that proton irradiation induced intergranular cracking in high purity 304L stainless steel in high-temperature water. The water environment was necessary for cracking to occur, as demonstrated by the absence of cracking in the irradiated region in the inert environment tests. As the irradiation of these specimens is intended to model the post irradiation microstructural and microchemical damage generated by neutrons under light water reactor conditions, the presence of cracking is of particular interest.

The role of chromium depletion in IASCC can be assessed by comparing the cracking susceptibility of the irradiated UHP specimens tested in water at 288°C to that of the unirradiated UHP specimen in the same environment. Severe cracking was found in the irradiated UHP specimens, where the chromium concentration at the grain boundary was depleted from the bulk concentration of 20.7 at% to 17.2 at% (Auger) or 17.3 at% (STEM/EDS). In the absence of grain boundary chromium depletion, no cracking was observed in the unirradiated UHP specimen. The measured grain boundary concentration in the irradiated UHP alloy is apparently rather high for such severe cracking to occur, when compared to concentrations of 15 at% required to cause significant cracking in thermally sensitized material [9]. However, the simultaneous radiation damage may act to raise the threshold concentration of grain boundary chromium at which intergranular SCC occurs. While it is likely that chromium depletion is necessary for cracking to occur, grain boundary chromium concentrations lower than those found in the UHP alloy were present in the UHP + P and UHP + Si alloys which were less susceptible to cracking. These results indicate that chromium depletion alone does not control the cracking process.

The role of phosphorus in IASCC can be examined by comparing the IGSCC susceptibility of the irradiated region to the unirradiated region of a UHP + P

specimen. The grain boundary phosphorus concentration in the unirradiated region due to thermal segregation of 5.3 at% was comparable to that found in the irradiated region of 8.7 at%, with both being over 50 times greater than the bulk concentration. The grain boundary phosphorus concentration of 5.3 at% in the unirradiated region of the UHP + P specimens did *not* induce cracking, indicating that the presence of phosphorus alone does not cause cracking. This is consistent with the previously mentioned results of Andresen and Briant [4,5]. The grain boundary chromium concentration of 15.0 at% (Auger) in the irradiated UHP + P specimen was lower than that of the grain boundary chromium concentration of 17.2 at% (Auger) in the irradiated UHP specimen, which cracked profusely. If phosphorus had no effect, or enhanced cracking, then even more cracks would be present due to the lower chromium concentration. However, the irradiated UHP + P specimens cracked much less than the irradiated UHP specimens, indicating that phosphorus is actually beneficial. Similar results were reported by Fukuya et al [8] in tests with high purity heats, where 50% IGSCC and an elongation at failure of 12% was found in a high purity specimen, compared to 13% IGSCC and an elongation at failure of 24% in a high purity specimen containing 0.0035 wt% phosphorus.

The role of silicon in IASCC can be assessed by comparing the cracking found after high temperature tests in the irradiated UHP + Si specimens with that found in the irradiated UHP specimens. Along with enrichment of the grain boundary silicon concentration to 3.2 at% (STEM/EDS) in the irradiated UHP + Si specimens we observed reduced cracking in the irradiated region, and increased elongation at failure when compared to the irradiated UHP alloy. These parameters indicate that the UHP + Si specimens were less susceptible to IGSCC than the irradiated UHP specimens, in a manner similar to that of the irradiated UHP + P specimens. The grain boundary chromium concentration as determined by STEM/EDS was significantly lower in the irradiated UHP + Si specimens (14.4 at%) than it was in the irradiated UHP specimens (17.3 at%), and the dislocation loop and black-dot densities were higher, yet the cracking susceptibility was apparently lower in the irradiated UHP + Si specimens. Thus the presence of silicon was apparently beneficial as it offset the detrimental effect expected due to the reduced chromium concentration. Little data is available for comparison, as no studies isolating the effect of silicon have been published. However, these results agree with those from Chung et al. [17] for neutron irradiated stainless steel, which suggested greater IGSCC resistance in a commercial purity alloy with a higher silicon concentration than a high purity alloy. They disagree with the earlier results of Jacobs et al. [16] which implicated silicon as detrimental in neutron irradiated stainless steel. As neither of these investigations could isolate the role of silicon, the present work is the first to suggest a beneficial effect of silicon in irradiated stainless steel.

The role of sulfur in the IASCC process could be examined by comparing the cracking susceptibility of the irradiated UHP + S specimens to the irradiated UHP specimens. However, the cracking susceptibility of the irradiated UHP + S specimens was not clear from these results, with two UHP + S specimens failing at low elongations (comparable to those of the irradiated UHP specimens), and the third failing at high elongation. It is possible that the high elongation specimen was compromised by the experimental problems previously mentioned. As the number of intergranular cracks in the irradiated region was low in all three specimens, the intergranular cracking susceptibility in the irradiated region is apparently low for this alloy. However, the transgranular cracking susceptibility seems comparable to the irradiated UHP alloy, such that failure occurs at elongations much lower than the unirradiated UHP specimen. The irradiated UHP + S specimens are the only ones in which the degree of intergranular cracking (determined by number of cracks) is inconsistent with the degree of transgranular cracking (determined by the reduction in elongation). Thus, there is insufficient data to conclusively identify an effect of sulfur in the present work.

Hydrogen remaining from the proton irradiation did not contribute significantly to the cracking found in the water tests, as suggested by the absence of cracking in the irradiated region of the irradiated UHP and UHP + P specimens tested in argon at high temperature or the irradiated UHP specimen tested in room temperature air. As the sensitivity of stainless steel to hydrogen cracking becomes greater with decreasing temperature, the absence of cracking at room temperature is especially significant. Further, the presence of phosphorus at the grain boundaries in hydrogen charged 316 stainless steels greatly enhanced cracking in CERT tests performed at cathodic potentials in 1N H_2SO_4 at room temperature, as found by Bruemmer et al. [26]. In our alloys, intergranular fracture in the unirradiated region was achieved at 0°C in only the hydrogen charged UHP + P Auger specimen, and not in hydrogen charged Auger specimens from the other alloys. These observations tend to support the contention that intergranular cracking would have been more severe in the irradi-

ated UHP + P specimens if hydrogen were a significant part of the cracking process. However, the lower amount of cracking after high temperature water SCC tests in the irradiated UHP + P specimens compared to cracking in the irradiated UHP specimens strongly suggests that hydrogen was not an important part of the cracking process during the high temperature water tests.

The hardening of the microstructure due to radiation-induced damage clearly had important implications for the deformation of these irradiated alloys. Prominent slip steps were found in the irradiated region of the highly deformed specimens which experienced minimal cracking, indicating that dislocation glide was confined to a relatively low number of preferred crystallographic planes. Such inhomogeneous slip is caused by the elimination of the irradiation induced microstructural defects by dislocation motion along specific planes, resulting in subsequent slip along these planes, or dislocation channeling [27]. The slip steps were less prominent in the irradiated specimens which exhibited severe cracking. This was due to two factors; the lower elongation experienced by these samples and the relief of stress in the irradiated layer caused by the extensive cracking. The greater degree of concentrated slip in the samples which experienced less cracking implies that dislocation channeling was not directly involved in the stress corrosion cracking of irradiated specimens. As cracking was not found on the irradiated UHP specimens strained in high temperature argon, hardening alone was not sufficient to cause cracking.

The severity of the cracking found in the irradiated UHP specimens at a higher grain boundary chromium concentration than that required for cracking in thermally treated material suggests that the increased susceptibility may be attributed in part to the difference in the hardness of the microstructure between the unirradiated and irradiated specimens. In an attempt to reproduce the microstructure and grain boundary chemistry due to irradiation, Jacobs [28] performed CERT tests in 2.5 pH water at 288°C on cold worked specimens with various thermal treatments designed to segregate phosphorus to the grain boundaries, and found up to 10% intergranular cracking. While these experiments indicate that hardening with phosphorus segregation can increase the cracking susceptibility of stainless steel specimens, the nature of the microstructure due to cold work is quite different from that due to irradiation, and the validity of comparing these experiments to those using irradiated specimens is unclear.

The microstructural variations *between* the irradiated alloys were apparently minor, with dislocation loop and black dot densities varying by approximately a factor of two over the four alloys examined. At present, there is no information relating the sensitivity of the cracking found to the variations in these parameters and it is difficult to attribute the differences in the severity of cracking to differences in the microstructure between the irradiated alloys.

As only 2% of the specimen thickness was irradiated, the microstructure was not homogeneous through thickness, and the measured strain at failure was not necessarily related to the IASCC susceptibility of the irradiated region. The cracking susceptibility of the irradiated specimens was principally assessed by the number of cracks in the irradiated region. Since the proton penetration depth is only 2% of the sample thickness, any effect of irradiation on the mechanical properties or intergranular cracking susceptibility was expected to be confined to the near-surface regions. This is confirmed by the large number of surface intergranular cracks on the irradiated specimens which extend only to the proton penetration depth. The striking difference in lateral contraction of the irradiated surface in fig. 9a is also expected from many studies on ion implantation which have shown that surface hardening (0.1–1 μm depth) can strongly affect the the nature of surface deformation [29,30]. However, the correlation of elongation at failure, (a bulk property), with the degree of cracking was not expected. As observed in fig. 10a–d, the initial stress–strain behavior of the irradiated specimens is not significantly different from their unirradiated counterparts because the bulk of the cross section (98%) was not affected by irradiation. But it appears that final failure is governed by the nucleation and propagation of the transgranular crack below the intergranular crack. Apparently, numerous intergranular cracks increase the probability of transgranular cracking, the propagation of which determines the elongation at failure. Therefore, the total elongation at failure appears to be related to the intergranular cracking susceptibility of the irradiated region, due to the nucleation and propagation of subsequent transgranular cracks in the bulk.

5. Conclusions

(1) The irradiation of ultrahigh purity (UHP) 304 stainless steel with 3.4 MeV protons caused severe intergranular cracking in CERT tests in high purity water at 288°C. The absence of cracking in identical specimens after argon CERT tests at 288°C demon-

strated that the environment was critical for cracking to occur. The presence of implanted hydrogen from the proton irradiation does not appear to contribute to the cracking observed in the irradiated specimens.

(2) Chromium depletion at the grain boundaries occurred in all of the irradiated alloys, whether undoped or doped with phosphorus, silicon, or sulfur. Although the irradiated alloys doped with phosphorus or silicon had lower grain boundary chromium concentrations than the irradiated UHP alloy, the cracking found in the doped specimens was not as severe as the cracking found on the undoped specimens. Thus it is likely that chromium depletion is necessary for cracking to occur, but does not alone determine the cracking susceptibility.

(3) The high grain boundary concentration of phosphorus in the irradiated UHP + P alloy, or silicon in the irradiated UHP + Si alloy, correlates with lower grain boundary chromium and less intergranular cracking, suggesting that these elements may be beneficial by mitigating the effect of chromium depletion.

(4) Although no sulfur segregation due to irradiation was found, the presence of sulfur correlates with less intergranular cracking, but the effect on the elongation at failure was not clear. Thus the role of sulfur could not be isolated from this study.

(5) The hardening of the microstructure in the irradiated alloys was clearly linked to the deformation of the irradiated specimens, and may contribute to the differences in the cracking behavior between the alloys. However, the observed variations in the irradiated microstructures did not suggest an obvious link between cracking and microstructure.

Acknowledgements

The authors would like to thank Dr. P.L. Andresen at General Electric for supplying the ultrahigh purity alloys and helpful discussions, Dr. J.R. Martin and the Cambridge Surface Science Facility at MIT, and Dr. E.A. Kenik and SHaRE program at Oak Ridge National Laboratories and Oak Ridge Associated Universities. We would also like to thank the Michigan Ion Beam Laboratory for Surface Modification and Analysis for proton irradiations, the High Temperature Corrosion Laboratory, and the Electron Microbeam Analysis Laboratory at the University of Michigan. This work was supported by the General Electric Co., and the Department of Energy, under grant DE-FG07-88ER-12825.

References

[1] P.L. Andresen, F.P. Ford, S.M. Murphy and J.M. Perks, Proc. 4th Int. Symp. on Environmental Degradation of Materials in Nuclear Power Systems - Water Reactors, Jekyll Island, GA, ed. D. Cubicciotti (National Association of Corrosion Engineers, 1990) p. 1-183.
[2] G.S. Was and P.L. Andresen, J. Metals 44 (1992) 8.
[3] P L. Andresen, Proc. 5th Int. Symp. on Environmental Degradation of Materials in Nuclear Power Systems - Water Reactors, Monterey CA, D. Cubicciotti ed. (American Nuclear Society, 1992) p. 209.
[4] P.L. Andresen and C.L. Briant, Corrosion 45 (1989) 443.
[5] C.L. Briant and P.L. Andresen, Metall. Trans. A19 (1988) 495.
[6] S.M. Bruemmer, E.P. Simonen and L.A. Charlot, Proc. 4th Int. Symp. on Environmental Degradation of Materials in Nuclear Power Systems - Water Reactors, Jekyll Island, GA, ed. D. Cubicciotti (National Association of Corrosion Engineers, (1990) p. 14-1.
[7] C.M. Shepherd, and T.M. Williams, Proc. 4th Int. Symp. on Environmental Degradation of Materials in Nuclear Power Systems - Water Reactors, Jekyll Island, GA, ed. D. Cubicciotti (National Association of Corrosion Engineers, 1990) p. 14-11.
[8] K. Fukuya, K. Nakata and A. Horie, Proc. 5th Int. Symp. on Environmental Degradation of Materials in Nuclear Power Systems - Water Reactors, Monterey CA, ed D. Cubicciotti (American Nuclear Society, 1992) p. 814.
[9] S.M. Bruemmer, B.W. Airey and L.A. Charlot. Proc. Corrosion '91 (National Association of Corrosion Engineers, 1991) paper 40.
[10] S.M. Bruemmer, Mater. Sci. Forum 46 (1989) 309.
[11] A.J. Sedriks, Corrosion of Stainless Steel (Wiley, New York, 1979).
[12] R.H. Jones, in Metals Handbook, 9th ed., vol. 13 (1987) p. 145.
[13] K. Asano, K. Nakata, K. Fukuya and M. Kodama, Proc. 5th Int. Symp. on Environmental Degradation of Materials in Nuclear Power Systems - Water Reactors, Monterey CA, ed. D. Cubicciotti (American Nuclear Society, 1992) p. 838.
[14] A.J. Jacobs, Proc. 16th Radiation Effects Conf. (ASTM, 1992), in press.
[15] M. Kodama, S. Nishimura, J. Morisawa, S. Shima, S. Suzuki and M. Yamamoto, Proc. 5th Int. Symp. on Environmental Degradation of Materials in Nuclear Power Systems - Water Reactors. Monterey CA, ed. D. Cubicciotti (American Nuclear Society, 1992) p. 948.
[16] A.J. Jacobs, J.E. Clausing, M.K. Miller and C.M. Shepherd, Proc. 4th Int. Symp. on Environments Degradation of Materials in Nuclear Power Systems - Water Reactors, Jekyll Island, GA, ed. D. Cubicciotti (National Association of COrrosion Engineers, 1990) p. 14-21.
[17] H.M. Chung, W.E. Ruther, J.E. Sanecki and T.F. Kassner, Proc. 5th Int. Symp. on Environmental Degradation of Materials in Nuclear Power Systems -Water Reactors,

Monterey CA, ed. D. Cubicciotti (American Nuclear Society, 1992) p. 795.
[18] K.T. Aust, Trans. Metall. Soc. AIME 245 (1969) 2117.
[19] J.M. Cookson, R.D. Carter, D.L. Damcott, M. Atzmon, G.S. Was and P.L. Andresen, Proc. 5th Int. Symp. on Environmental Degradation of Materials in Nuclear Power Systems – Water Reactors, Monterey CA, ed. D. Cubicciotti (American Nuclear Society, 1992) p. 806.
[20] P.R. Okamoto and L.E. Rehn, J. Nucl. Mater. 83 (1979) 2.
[21] J.F. Ziegler and J.P. Biersack, TRIM 90 program, (IBM Corp., Yorktown, NY, 1990.
[22] C.L. Briant, Metall. Trans. A16 (1985) 2061.
[23] L.E. Davis, N.C. MacDonald, P.W. Palmberg, G.E. Riach and R.E. Weber, Handbook of Auger Spectroscopy (Physical Electronics Division, Perkin-Elmer Corp., Eden Prairie, MN, 1978).
[24] D.L. Damcott, R.D. Carter, J.M. Cookson, M. Atzmon, G.S. Was and J.R. Martin, Radiat. Eff. Def. Solids 118 (1991) 383.
[25] R.D. Carter, Jr., D.L. Damcott, M. Atzmon and G.S. Was, J. Nucl. Mater., in press.
[26] S.M. Bruemmer, L.A. Charlot, E.P. Simonen, Proc. Corrosion '90 (National Association of Corrosion Engineers. 1990) paper 506.
[27] E.E. Bloom, W.R. Martin, J.O. Stiegler and J.R. Weir, J. Nucl. Mater. 22 (1967) 68.
[28] A.J. Jacobs, Corrosion, 46 (1990) 30.
[29] G.K. Hubler, in Surface Alloying by Ion, Electron and Laser Beams, eds. L.E. Rehn, S.T. Picraux and H. Wiedersich (American Society for Metals, 1987) p. 287.
[30] J.K. Hirvonen and C.R. Clayton, in: Surface Modification and Alloying, eds. J.M. Poate, G. Foti and D.C. Jacobson NATO Conf. Series, Series VI: Materials Science, part 8 (1983) p. 323.